PHYSICAL REVIEW B VOLUME 43, NUMBER 14 15 MAY 1991-I

Temperature dependence of the dielectric function and the interband critical-point parameters of $Al_xGa_{1-x}As$

S. Logothetidis,* M. Cardona, and M. Garriga
Max-Planck-Institut für Festkörperforschung, Heisenbergstrasse 1, D-7000 Stuttgart 80, Germany
(Received 16 November 1990)

The complex dielectric function $\epsilon(\omega)$ of $Al_xGa_{1-x}As$ was studied in the 1.4–5.6-eV photon energy region and between 12 and 800 K. By performing a line-shape analysis of the observed structures, the temperature dependence of the interband critical-point energies, broadenings, strength, and excitonic phase angle have been determined. The compositional dependence of these parameters was also obtained, e.g., the temperature dependence shift of the E_0 exciton and E_1 transitions was found to be $5.5+3.35x$ (10^{-4} eV/K). The decrease (increase) in energy (broadening) with increasing temperature was analyzed in terms of average phonon frequencies, giving rise to renormalization of the energies and a broadening of the band gaps. The statistical fluctuation of the alloy composition, which appears as an additional broadening, was found to affect the E_0, $E_0+\Delta_0$, E_1, and $E_1+\Delta_1$ structures. The excitonic character of the E_1 and $E_1+\Delta_1$ transitions shows a systematic change from a localized Lorentzian to two-dimensional character with increasing both Al content and temperature. The E_2 structure [E_0', $E_2(X)$, $E_2(\Sigma)$, and $E_2(P)$ transitions] was found to change its strength and to increase in complexity by going from the Ga- to the Al-rich regime.

I. INTRODUCTION

The alloy system $Al_xGa_{1-x}As/GaAs$ is of great technological importance for high-speed electronic and optoelectronic devices due to the nearly perfect lattice match of GaAs or AlAs.[1] However, a small misfit strain corresponding to the small lattice constant differences is generated in the deposited epilayer and gives measurable effects on the physical properties of the layers.[1–4] The band-gap energy of $Al_xGa_{1-x}As$ and its dependence on the alloy composition are known to be among the most important device parameters. Hence considerable attention has been focused on the study of the direct gap E_0 at the Γ point (Γ_8^v-Γ_6^c),[5] on the indirect gap between X and Γ points (Γ_8^v-X_6^c),[6,7] and on the crossover of the conduction-band minimum at the X and Γ points occurring for $x \approx 0.45$.[8–10] The random distribution of Al and Ga atoms at cation sites in $Al_xGa_{1-x}As$ alloys implies phenomena not found in binary III-V semiconductors. The induced statistical potential fluctuations result in changes in the alloy's physical properties. More specifically, a nonlinear dependence of the band gaps on alloy composition x is observed[2,3,6,11–13] while disorder effects due to alloy scattering produce an additional broadening of the electronic states.[14–19]

A knowledge of the fundamental optical properties of their components is often required for the design of electronic devices. For many applications of the $Al_xGa_{1-x}As$ alloys their dielectric behavior must be known. The macroscopic linear optical response of the material is represented by the dielectric function $\epsilon(\omega)$ ($\epsilon_1+i\epsilon_2$) which is closely related to the electronic band structure of the material. The structure observed in the $\epsilon(\omega)$ spectra is usually attributed to interband critical points (CP's) which can be analyzed in terms of standard analytic line shapes:[20,21]

$$\epsilon(\omega)=C-Ae^{i\phi}(\omega-E+i\Gamma)^n , \quad (1)$$

where a critical point is described by the amplitude A, the threshold energy E, the broadening Γ, and the excitonic phase angle ϕ. The exponent n has the value $-\frac{1}{2}$ for one-dimensional (1D), $\alpha \rightarrow 0$ for 2D [logarithmic line shape, i.e., Eq. (1) should be replaced by a $\ln(E-\omega-i\Gamma)$], and $\frac{1}{2}$ for 3D CP's. Discrete excitons are represented by $n=-1$. The CP's are directly related to regions of large or singular joint density of electronic states. Hence the CP's yield direct information about the energy separation of the valence and conduction bands (interband gaps) which can be compared with band-structure calculations.[22]

Spectroscopic ellipsometry (SE) is an excellent technique to investigate the dielectric function and the interband transitions.[12,21,23,24] In the past few years our group has been engaged in the systematic investigation of the dependence of the critical-point parameters on temperature of a series of group-IV materials[25–27] and III-V compounds[24,28,29] utilizing this technique. In parallel with this experimental work, a theoretical description for the renormalization of the energy bands of these semiconductors through the electron-phonon interaction has been developed which describes the energy shifts as the real part of the self-energy and the broadening of states through the imaginary part of the self-energy.[30–33]

The $Al_xGa_{1-x}As$ system shows a complex conduction-band diagram. Figure 1 shows the band structure of GaAs and AlAs calculated within the self-consistent scalar relativistic linear muffin-tin method (LMTO),[22,34] including the location of several direct interband transitions at different parts of the Brillouin zone (BZ). The fundamental absorption edge of GaAs (E_0) is

 ©1991 The American Physical Society

dominated by the edge exciton, about 4.2 meV (Ref. 35) lower than the direct band gap E_0 which is located at the Γ point of the BZ. For the fundamental gap in $Al_xGa_{1-x}As$ a transition is observed from a direct to an indirect gap at the composition $x \simeq 0.45$,[1,8] whereas the lower conduction-band minima undergo a crossover from the sequence Γ-L-X in GaAs to X-L-Γ in AlAs.[8-10] The second lowest interband critical point $E_0+\Delta_0$ corresponds to transitions from the spin-orbit-split valence band to the lowest conduction band at the Γ point. At higher energies the assignment of observed interband transitions to critical points in the BZ for GaAs is now well established.[22,24,36,37] Thus the structures labeled as E_1 and $E_1+\Delta_1$ take place along the Λ lines of the BZ ($\langle 111 \rangle$ directions), whereas the most prominent structures in the energy region from 4 to 5.5 eV have been identified as E_0' at the Γ point and $E_2(\Sigma)$ including an extended region in the ΓXUL plane.[22,36] Weaker structures, in GaAs, in the region of E_0' transition have been identified as $E_0'+\Delta_0'$ at the Γ point and Δ direction,[37] while the weak structure very close to $E_2(\Sigma)$ at 4.9 eV, labeled $E_2(X)$, has been attributed to $X_7^v \rightarrow X_6^c$ transitions. On the other hand, for AlAs and the $Al_xGa_{1-x}As$ alloys, due to the lack of accurate experimental data and the complexity of the spectra obtained with increasing x the assignment is less certain.

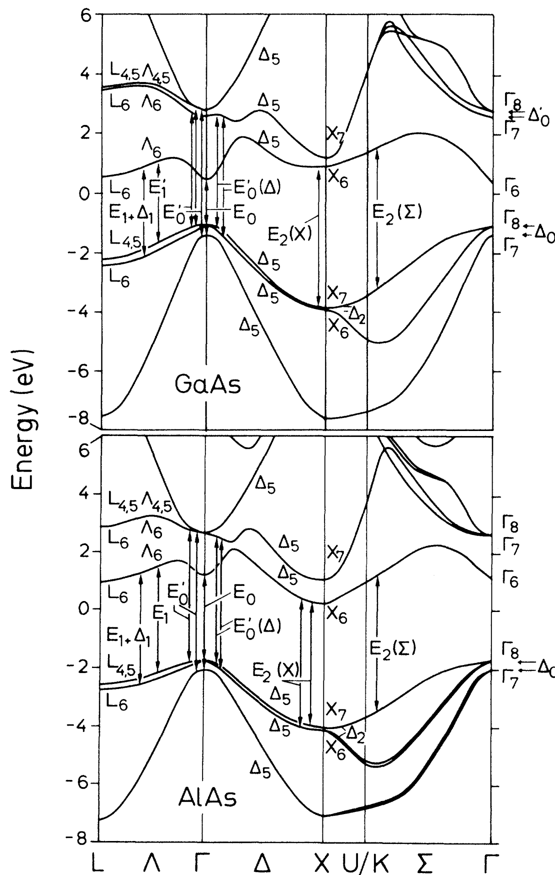

FIG. 1. Band structure of (a) GaAs and (b) AlAs reproduced from Ref. 34. The interband critical points relevant to this work are indicated by arrows.

Relatively little work has been done on the optical properties of the $Al_xGa_{1-x}As$ alloy system. The dielectric function of $Al_xGa_{1-x}As$ alloys[12] and AlAs (Ref. 38) has been studied ellipsometrically between 1.5 and 6 eV at room temperature. In both these works there are no conclusive identifications of the critical points which give rise to interband transitions in the E_2 energy region. Electroreflectance measurements on the various interband transitions in $Al_xGa_{1-x}As$ alloys[11] and AlAs (Ref. 39) have been carried out at room temperature. Adachi[40] has expressed the dielectric function of $Al_xGa_{1-x}As$ alloys in analytical form by using data of Ref. 12 and a simplified model of the band structure of the materials.

In the earlier paper[34] we have presented an identification of interband transitions of $Al_xGa_{1-x}As$ alloys and AlAs in the energy region from 4 to 5.5 eV. This identification has been accomplished by analyzing the dielectric function measurements obtained at low temperatures by SE in a number of $Al_xGa_{1-x}As$ and AlAs samples and by using the calculated band structures and dielectric functions of pure GaAs and AlAs. In Ref. 34 we have reassigned the structure previously attributed to E_2 from the ΓXUL $[E_2(P)]$ as $E_2(\Sigma)$ and vice versa. Also, we have found that an inversion of the relative strengths of the $E_2(P)$ and $E_2(\Sigma)$ transitions takes place in going from GaAs to rich Al content, which was attributed to changes in the parallelism of the bands.

In this paper we apply the SE technique to investigate the temperature dependence of the dielectric function and the interband critical-point parameters of $Al_xGa_{1-x}As$ alloy in the temperature range between 15 and 800 K and energy range from 1.4 to 5.6 eV. We present data for the E_0, $E_0+\Delta_0$, E_1, E_0', and E_2 transitions for three different Al compositions. In Sec. II we describe the experimental setup, in Sec. III we present the results for our analysis for several interband transitions. The results are discussed in Sec. IV. As usual, we observe a decrease (increase) of the CP energies (broadenings) with increasing temperature. Emphasis is given to the compositional dependence of the CP broadenings observed at low temperatures as well as to the character of the E_1 and $E_1+\Delta_1$ transitions and their dependence on both temperature and Al content.

II. EXPERIMENT

$Al_xGa_{1-x}As$ layers with thicknesses ranging from 1 to 5 μm were grown by liquid-phase epitaxy (LPE). They are n-type undoped epitaxial layers grown on a semi-insulating GaAs(001) substrate. The aluminum content x was estimated from x-ray studies and from E_0 and E_1 energy gaps at room temperature found from ellipsometric measurements according to Ref. 12.

Spectroscopic ellipsometry measurements were performed with an automatic spectral ellipsometer, essentially the same as that described in Ref. 25. Before mounting the sample into the cryostat, a wet-chemical etching was carried out in order to obtain the largest dielectric discontinuity between sample and ambient. This can be

conveniently done by maximizing the $\epsilon_2(\omega)$ value in the E_2 energy region, which is the most sensitive one to the presence of overlayers. To optimize the ϵ_2 at E_2 we followed the etching procedure described in Ref. 12. During this procedure the sample was kept at room temperature in a windowless glass box in flowing dry N_2. After etching, the sample was placed in the cryostat which was also closed in a N_2 atmosphere. The cryostat used has been described in Ref. 24. The sample temperature was determined with three appropriately calibrated iron-constantan thermocouples and the temperature stability was typically ± 3 K up to 80 K and ± 1 K at higher temperatures. During the low-temperature measurements the vacuum was better than 10^{-8} Torr and slightly worse at higher temperatures. The energy spacing of the experimental points were (a) in the exciton region 1, 2, and 5 meV (with a spectral slit width better than 1 meV) and (b) 10 meV in the higher-energy region. All the spectra were taken at an angle of incidence of 67.5°.

III. RESULTS

Spectroscopic ellipsometry measures the complex reflection ratio $\rho = r_p / r_s$, between the Fresnel reflection coefficients r_p and r_s at a given angle of incidence θ and energy ω.[41] In the case where a perfect discontinuity exists between the measured cubic material and the ambient material (two-phase model), the dielectric function $\epsilon(\omega)$ is directly related to the measured ratio ρ. However, an oxide overlayer grows when the material is exposed to the atmosphere (during the transfer of the sample to the cryostat and the outgassing process after the chemical treatment) for a period of time. The presence of an oxide layer is indicated mainly by a decrease of the value of ϵ_2 at E_2, interpreted in the two-phase model. Within a three-phase model (air oxide of GaAs-$Al_xGa_{1-x}As$) and using the dielectric function of the oxide given in Ref. 42, we calculate the film thickness to be about 8 Å.

In Fig. 2 we show the real and imaginary parts of the dielectric function of $Al_{0.27}Ga_{0.53}As$ for several temperatures after introducing the 8-Å oxide correction mentioned above. The main structures below 4 eV correspond to the E_0, $E_0+\Delta_0$, E_1, and $E_1+\Delta_1$ interband transitions, whereas E_0' and E_2 contribute to the structure at higher energies. An energy shift and broadening of the spectral structures are observed with increasing temperature. Similar results are obtained for other Al compositions ($x = 0.53$ and 0.69), where the structure around 4.5 eV is mainly due to the E_2 transition. In order to obtain the CP parameters, the second or third derivatives of the dielectric spectra were numerically calculated. The structure so enhanced was fitted to excitonic or two-dimensional critical-point line shapes [Eq. (1)].

Figure 3 shows the experimental second-derivative spectra of ϵ_1 for three Al compositions ($x = 0.27$, 0.53, and 0.69) in the spectral region around the E_0 and $E_0+\Delta_0$ structures. The lines represent the best fits to excitonic line shapes [Eq. (1) for $n=-1$]. In this region of the spectra the fits were performed only for the real part of the dielectric function because of the poor sensitivity of our ellipsometer to changes in the ϵ_2 value around the fundamental gap which leads to rather noisy derivatives of ϵ_2. Also, the experimental data points shown in Fig. 3 were taken with a 5-meV energy step which is large in comparison with the structure broadening at temperatures lower than 300 K, as we will discuss later.

The region around E_1 and $E_1+\Delta_1$ was fitted to 2D line shapes [the logarithmic version of Eq. (1)]. Figure 4 shows the results for the second-derivative spectra of the samples mentioned above together with the best-fit line shapes. The structure in the region of the E_0' and E_2 transitions (Fig. 5) was also fitted to 2D line shapes. All the spectra shown in Figs. 3–5 were obtained between 12 and 22 K, except for the AlAs sample which was measured at 80 K.

In Fig. 6 we plot the temperature dependence of the exciton energies E_0 and $E_0+\Delta_0$ of $Al_xGa_{1-x}As$, for $x = 0.27$, 0.53, and 0.69, obtained by the procedure just mentioned. We also show in Fig. 6 the variation with temperature of the E_0 transition of GaAs.[24] The data in Fig. 6 have been fitted with two different functions. One of them (solid lines in Fig. 6) is based on the theory of the temperature shift of the gap produced by electron-phonon interaction,[24,32] and is given by

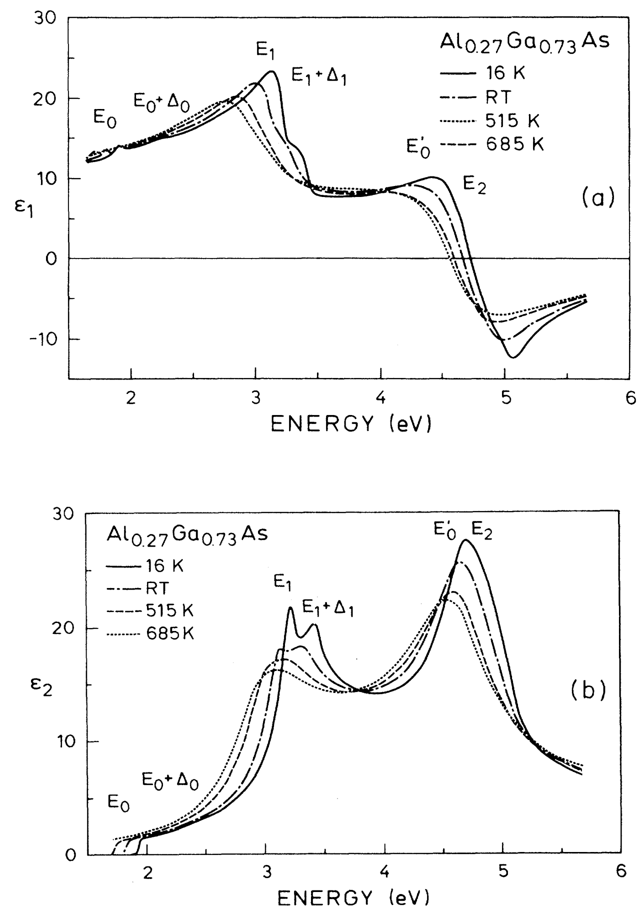

FIG. 2. (a) Real part and (b) imaginary part of the dielectric function $\epsilon_1 + i\epsilon_2$ of $Al_{0.27}Ga_{0.73}As$ for several temperatures.

$$E(T)=E_B-a_B(2n_B+1)\ ,$$
$$n_B=(e^{\Theta/T}-1)^{-1} \tag{2}$$

where Θ is a temperature related to an average phonon frequency. The other corresponds to the phenomenological expression

$$E(T)=E(0)-\frac{\alpha T^2}{T+\beta}\ , \tag{3}$$

proposed by Varshni.[43] The parameters of the fits with Eqs. (2) and (3) are listed in Table I.

The linewidths of critical points versus temperature are usually described with an expression similar to Eq. (2):

$$\Gamma(T)=\Gamma_1+\Gamma_0 n_B\ , \tag{4}$$

where Γ_1 represents the broadening due to additional temperature-independent mechanisms (Auger processes, electron-electron interaction, impurities, surface scattering, and also instrumental effects). Equation (4) is based on the assumption of broadening by interband scattering via phonon absorption and holds only for the lowest gap. For the other gaps one has to replace n_B in the above expression with $2n_B+1$ since now both phonon absorption and emission processes can take place. Figure 7 shows the broadening obtained from our line-shape analysis for the E_0 exciton in $Al_xGa_{1-x}As$ as a function of temperature for different x. The temperature dependence of the E_0 broadening of GaAs (Ref. 24) is also shown (dashed line). The scatter in the data of Fig. 7 suggests that a linear equation

$$\Gamma(T)=\Gamma_L+\gamma T \tag{5}$$

may equally well describe the behavior of the E_0 broadening in the whole temperature range. The parameters and their corresponding uncertainties obtained by fitting the data in Fig. 7 to Eqs. (4) and (5) are listed in

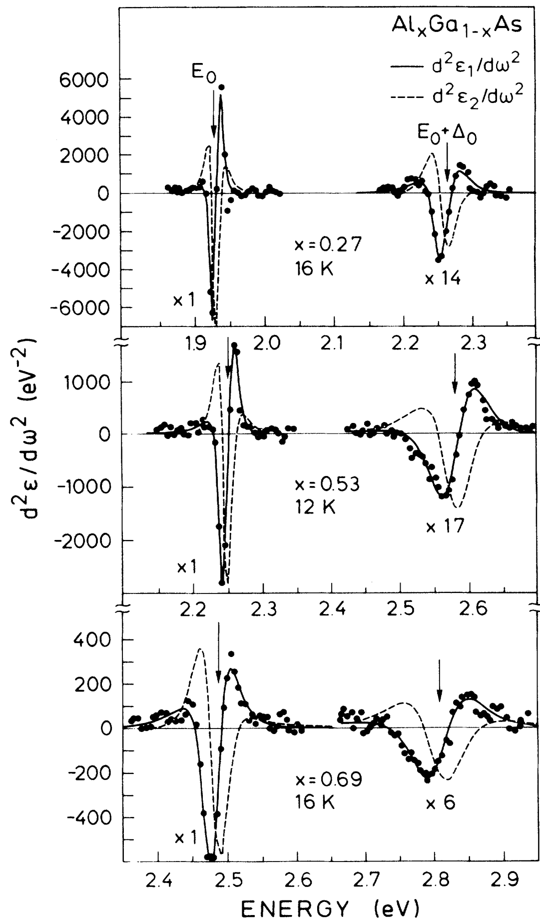

FIG. 3. Fits to the second derivatives of the real (solid lines) and imaginary (dashed lines) parts of the dielectric function of $Al_xGa_{1-x}As$ around the E_0 and $E_0+\Delta_0$ structures at low temperatures. The dots represent experimental data for $d^2\epsilon_1/d\omega^2$. Note the different energy scales and that the vertical scale has to be divided by the factor given under each structure.

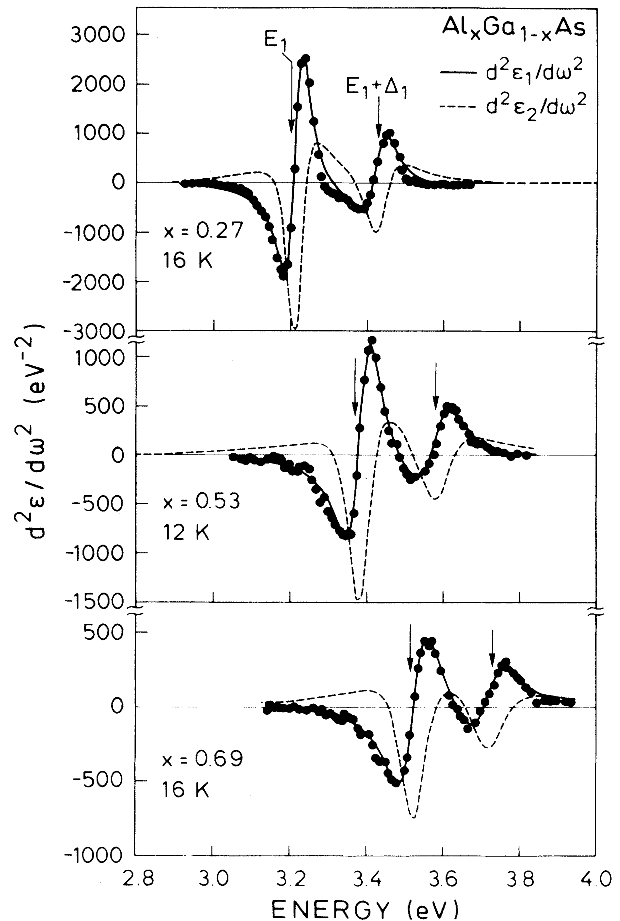

FIG. 4. Fits to the second derivatives of the real (solid lines) and imaginary (dashed lines) parts of the dielectric function of $Al_xGa_{1-x}As$ around the E_1 and $E_1+\Delta_1$ structures at low temperatures. The solid circles represent experimental data for $d^2\epsilon_1/d\omega^2$ (those for $d^2\epsilon_2/d\omega^2$ are not shown but the quality of the fit is similar).

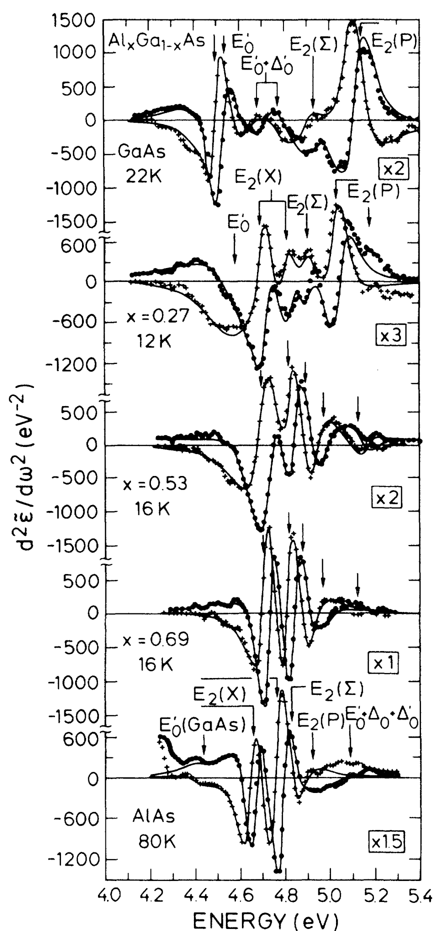

FIG. 5. Second derivatives of the real (crosses) and imaginary (circles) parts of the dielectric function of GaAs, $Al_xGa_{1-x}As$, and AlAs around the E_2 region at low temperatures. The solid lines are fits to the critical-point line shapes. Note that the vertical scale has to be divided by the factor given at the right of each spectrum.

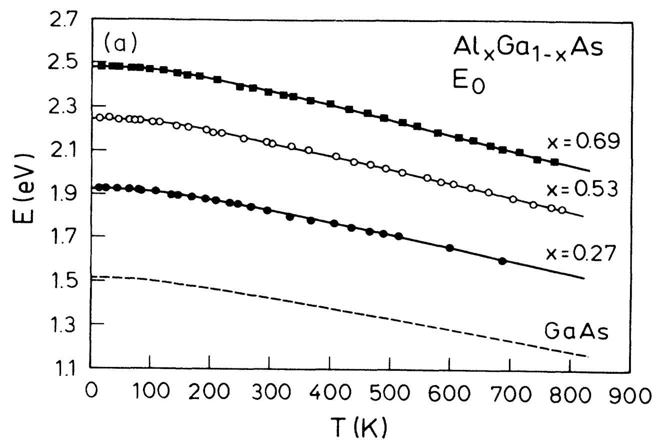

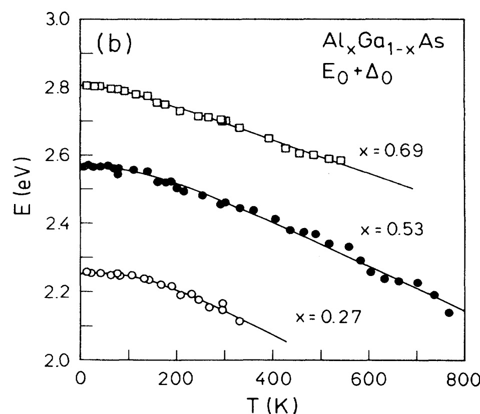

FIG. 6. Temperature dependence of the (a) E_0 and (b) $E_0+\Delta_0$ energies of $Al_xGa_{1-x}As$. The solid straight lines represent the best fits with Eq. (2). The fit parameters are given in Table I. The dashed line in (a) gives the temperature dependence of the E_0 energies of GaAs from Ref. 24.

TABLE I. Values of E_B, a_B, and Θ parameters obtained by fitting the E_0 and $E_0+\Delta_0$ critical-point energies vs temperature with Eq. (2), and values of $E(0)$, α, and β obtained by fitting the same data with Eq. (3). The numbers in parentheses indicate error margins.

	x	E_B (eV)	a_B (meV)	Θ (K)	$E(0)$ (eV)	α (10^{-4} eV K^{-1})	β (K)
	0	1.571(23)[a]	57(29)[a]	240(102)[a]	1.517(8)[a]	5.5(1.3)[a]	225(174)[a]
	0.18				1.771(7)[b]	6.3(5)[b]	236(73)[b]
E_0	0.27	2.011(10)	85(11)	295(32)	1.932(3)	6.48(40)	248(54)
	0.53	2.347(9)	104(11)	326(29)	2.251(3)	7.04(26)	261(38)
	0.69	2.401(12)	122(13)	355(31)	2.485(3)	7.88(36)	302(49)
	0	1.907(9)	58(7)	240(fixed)	1.851(5)	3.5(4)	255(fixed)
$E_0+\Delta_0$	0.27	2.399(9)	147(88)	390(135)			
	0.53	2.689(4)	127(45)	379(106)	2.567(10)	8.38(1.74)	435(238)
	0.69	2.846(14)	43(17)	175(62)	2.808(6)	5.22(56)	117(70)

[a]Reference 24.

[b]H. Shen, S. H. Pan, Z. Hang, and F. H. Pollak, Appl. Phys. Lett. 53, 1080 (1988).

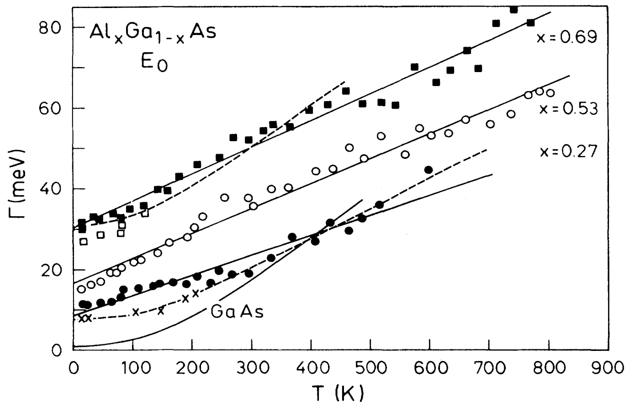

FIG. 7. Temperature dependence of the broadening of E_0 in $Al_xGa_{1-x}As$. The solid lines represent fits with a linear expression of the broadenings obtained by analyzing spectra with an energy step of 5 meV. The solid line labeled GaAs is a fit of the broadening data for GaAs from Ref. 24 with Eq. (4). Crosses for $x=0.27$ and open squares for $x=0.69$ represent the broadenings obtained by fitting spectra with an energy step of either 1 or 2 meV. The dashed lines for $x=0.27$ and 0.69 represent fits with Eq. (4). The fit parameters are given in Table II.

Table II.

The statistical fluctuation of the alloy composition, which is caused by the random distribution of Al and Ga on the cation sites, is responsible for an additional "inhomogeneous" broadening of the band-gap energy which can be estimated from a model proposed by Schubert *et al.*,[15]

$$\Gamma_a(x)=2.36\frac{dE}{dx}\left[\frac{x(1-x)}{KV(x)}\right]^{1/2}, \tag{6}$$

where dE/dx is the rate of band-gap variation with alloy composition, $K=4/a_0^3$ is the cation density, and $V(x)$ is the minimum scattering volume. This model has been successfully applied to the alloy broadening observed in photoluminescence spectra of ternary alloys such as $Al_xGa_{1-x}As$,[15] $Ga_xIn_{1-x}As$,[44] and $Cd_xHg_{1-x}Te$,[42] and generally to interpret the alloy broadening of the E_0 gap[18,19] of ternary alloys. One assumes that this alloy broadening $\Gamma_a(x)$ is temperature independent[15,19] and is simply added to the Γ_1 and Γ_L terms of expressions (4) and (5), respectively.

In the region around the E_1 and $E_1+\Delta_1$ transitions (Fig. 4) the second-derivative spectra were fitted to 2D line shapes. At every temperature the two structures were fitted simultaneously up to 500 K for $x=0.27$, 450 K for $x=0.53$, and 330 K for $x=0.69$. Figure 8 shows the temperature dependence of the E_1 and $E_1+\Delta_1$ CP energies of $Al_xGa_{1-x}As$ obtained in this fashion. The dashed line in the upper part of this figure represents the dependence of the E_1 CP of GaAs.[24] The data of Fig. 8 were fitted to Eqs. (2) and (3). The resulting parameters are listed in Table III. We can see from Fig. 8 and Table III that there are no significant differences in the energy dependence on temperature of the E_1 and $E_1+\Delta_1$ structures. The energies of the two structures run almost parallel and the spin-orbit splitting for all Al compositions is found to be temperature independent, as expected for an atomiclike property. Figure 9 shows the broadening of the E_1 and $E_1+\Delta_1$ structures versus temperature. Also in this figure the dashed line represents the temperature dependence of the E_1 broadening of GaAs (Ref. 24) that was fitted with a 2D line shape.

In order to complete the description of the CP parameters of the E_1 and $E_1+\Delta_1$ transitions of $Al_xGa_{1-x}As$ and to compare them for different Al content we plot in Figs. 10 and 11 the dependence of the strength A and the phase angle ϕ on temperature, respectively.

The region between 4 and 5.5 eV of the low-temperature spectra (Fig. 5) is complex and rich in structure,[34,37] where the number and character of resolved

TABLE II. Values of the parameters obtained by fitting the broadening Γ of the E_0 and $E_0+\Delta_0$ critical points of $Al_xGa_{1-x}As$ vs temperature to Eq. (4) or Eq. (5). The numbers in parentheses indicate error margins.

	x	Γ_1 (meV)	Γ_0 (meV)	Θ (K)	Γ_L (meV)	γ (10^{-4} eV K^{-1})	Temperature range (K)
E_0	0	1(2)[a]	48(30)[a]	430(240)[a]			20–300
	0.27	13.8(14)	51.6(15)	615(210)	8.5(1.8)	0.49(6)	15–600
		12(4)	18.2(9)	295(fixed)			15–600
		7.3(6)[b]	27(14)[b]	340(150)[b]			15–600
	0.53				16.6(1.5)	0.61(3)	12–800
	0.69	36.1(8)	27.4(2)	355(fixed)	30.3(1.8)	0.66(4)	16–750
		31(5)[c]	42(3)[c]	335(fixed)[c]			16–460
$E_0+\Delta_0$	0						
	0.27				29(2)	0.66(14)	15–350
	0.53	37(24)[d]	37(26)[d]	449(215)[d]	64.6(4)	1.17(13)	12–600
	0.69				44.5(7.2)	1.78(29)	16–500

[a]Reference 24.
[b]Values obtained below 300 K by analyzing spectra with an energy step of either 1 or 2 meV.
[c]Values obtained below 120 K by analyzing spectra with an energy step of 2 meV.
[d]The results fitted with the expression $\Gamma(T)=\Gamma_1+\Gamma_0(2n_B+1)$.

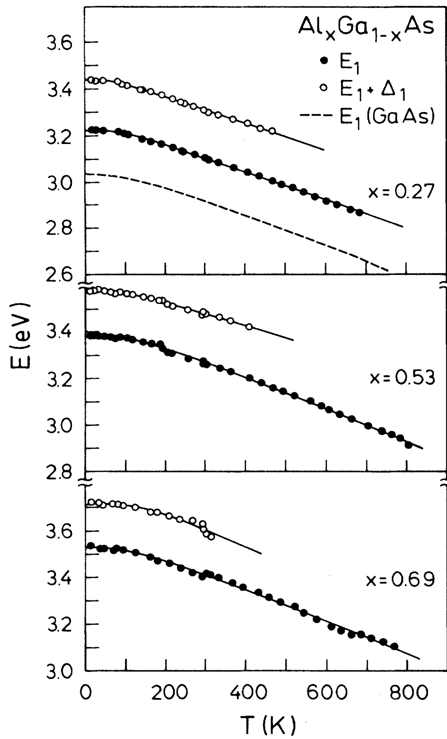

FIG. 8. Temperature dependence of the E_1 and $E_1+\Delta_1$ energies of $Al_xGa_{1-x}As$. The solid lines represent fits with Eq. (2). The fit parameters are given in Table III.

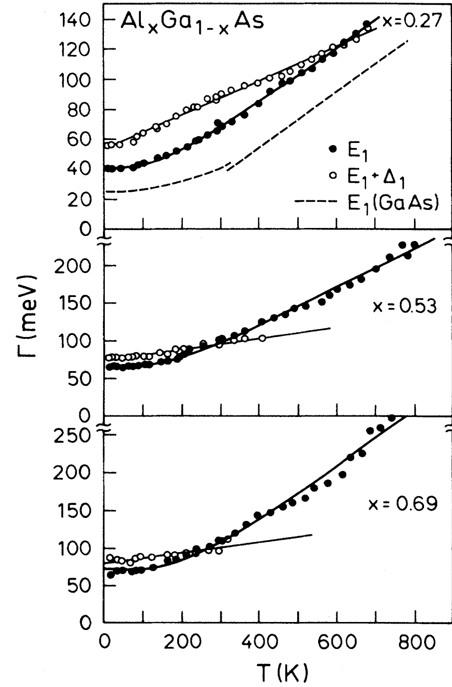

FIG. 9. Temperature dependence of the E_1 and $E_1+\Delta_1$ broadening of $Al_xGa_{1-x}As$. The solid lines represent fits with Eqs. (4) and (5). The fit parameters are given in Table VI. The dashed line represents the E_1 broadening of GaAs from Ref. 24 obtained by fitting the experimental data between 300 and 760 K with a 2D line shape.

CP's depends on the alloy composition. With increasing temperature the structures broaden and weak features observed in the low-temperature spectra "disappear" under the main structures, hindering a detailed analysis of the temperature behavior in this region. The two main structures E_0' and $E_2(X)$ for $x=0.27$ could be fitted together in the whole temperature range (solid circles in Fig. 12). Below 250 K, however, a model with three CP's [E_0', $E_2(X)$, and $E_2(X)+\Delta_2$] gave a better description of the derivative spectra (open symbols in Fig. 12). The difference in the two values of $E_2(X)$ in Fig. 12 is due to the fact that the $E_2(X)$ value for the two-CP case is the weighted average of the $E_2(X)$ and the weak $E_2(X)+\Delta_2$ structures.

In the $x=0.53$ case (Fig. 13) the spectra were fitted with three different models: (a) only one CP [$E_2(X)$], (b) with two CP's [$E_2(X)$ and $E_2(X)+\Delta_2$], and (c) with three CP's [$E_2(X)$, $E_2(X)+\Delta_2$, and $E_2(\Sigma)$]. Finally, for the spectra of the $x=0.69$ sample a model with three CP's [$E_2(X)$, $E_2(X)+\Delta_2$, and $E_2(\Sigma)$] was used through the whole temperature range.

It should be mentioned that although a model with three CP's usually gives the best description of the low-temperature spectra, the increasing broadening of the

TABLE III. Values of parameters obtained by fitting the E_1 and $E_1+\Delta_1$ critical-point energies vs temperature with Eqs. (2) and (3). The numbers in parentheses indicate error margins.

	x	E_B (eV)	a_B (meV)	Θ (K)	$E(0)$ (eV)	α (10^{-4} eV K^{-1})	β (K)	Line shape
E_1	0	3.125(9)[a]	91(11)[a]	274(30)[a]	3.041[a]	7.2(2)[a]	205(31)[a]	Excitonic and 2D
	0.27	3.296(6)	72(8)	235(23)	3.230(3)	6.62(19)	171(25)	2D
	0.53	3.491(10)	106(12)	308(30)	3.393(3)	7.55(33)	241(44)	2D
	0.69	3.641(21)	113(25)	324(59)	3.534(7)	7.8(6)	270(86)	2D
$E_1+\Delta_1$	0.27	3.486(8)	46(10)	158(32)	3.446(5)	6.04(44)	97(42)	2D
	0.53	3.649(16)	70(18)	261(49)	3.583(3)	6.86(90)	295(100)	2D
	0.69	3.898(18)	184(60)	439(236)				2D

[a]These parameters were obtained in Ref. 24 by using the energies fitted with excitonic line shapes up to 300 K and 2D line shape between 300 and 760 K.

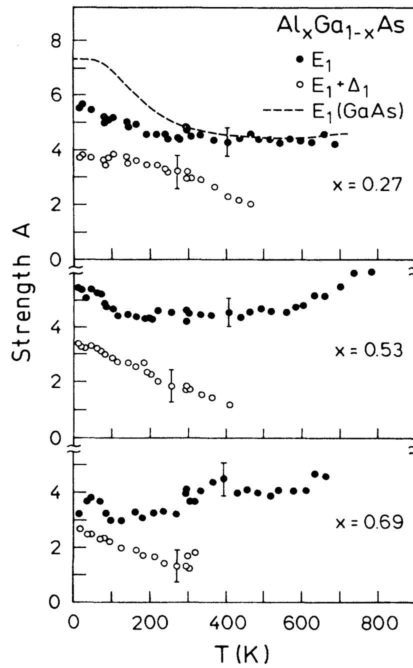

FIG. 10. Temperature dependence of the amplitudes of the E_1 and $E_1+\Delta_1$ structures of $Al_xGa_{1-x}As$ fitted with a 2D line shape. The temperature dependence of the E_1 amplitude of GaAs (dashed line) is from Ref. 24.

structures with increasing temperature results in smeared out peaks and the fit parameters tend to be more and more correlated, losing their meaning. Therefore a model with one or two CP's may be more suitable to describe the high-temperature behavior.

The temperature dependence of the energies and broadenings resulting from the different models used to fit the derivative spectra in the 4–5.5-eV energy region have been fitted to Eqs. (2)–(5). The best values for the fitting parameters are given in Table IV (energies) and Table V (broadenings).

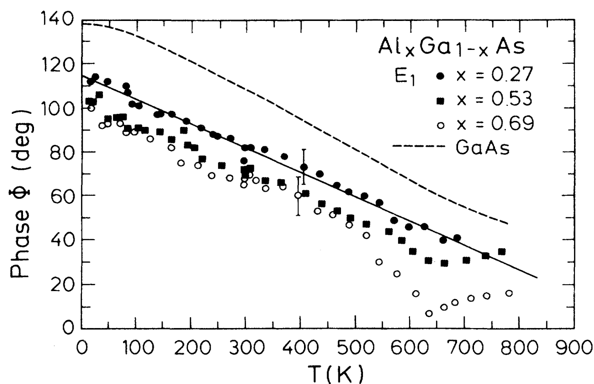

FIG. 11. Temperature dependence of the phase angle ϕ of the E_1 structure fitted with a 2D line shape. The dashed line gives the phase angle of the E_1 of GaAs after Ref. 24. The solid line is drawn as a guide to the eye.

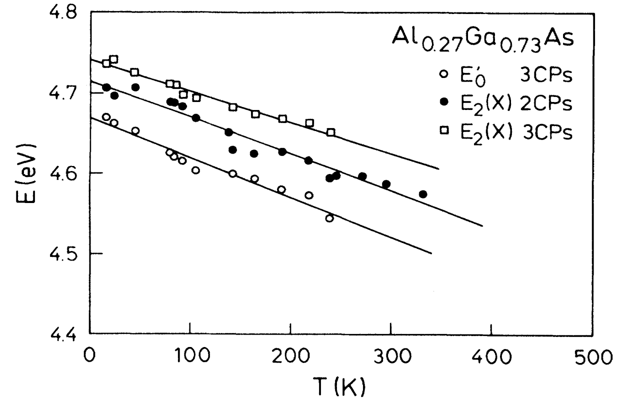

FIG. 12. Temperature dependence of the E_0' and $E_2(X)$ critical-point energies of $Al_{0.27}Ga_{0.73}As$. The solid lines represent linear fits. The fit parameters are given in Table IV. The results for the $E_2(X)$ structure were obtained by fitting the whole E_2 structure with two CP's (solid circles) or with three CP's (open squares).

IV. DISCUSSION

A. Edge excitons and $E_0+\Delta_0$ transitions

The lowest direct gap E_0 in $Al_xGa_{1-x}As$ is the excitonic transition between the fourfold degenerated Γ_8 valence band and the twofold Γ_6 conduction band. In the strained material the degeneracy of the valence band is partially lifted.[45,46] This results in a splitting of the E_0 excitonic transition. We have found[4,19] that the small lattice mismatch between the LPE $Al_xGa_{1-x}As$ layers and the GaAs substrate produces an observable splitting of the excitonic recombination given by $\delta E_S(x)=11.8x$ meV. A detailed discussion of this splitting and its tem-

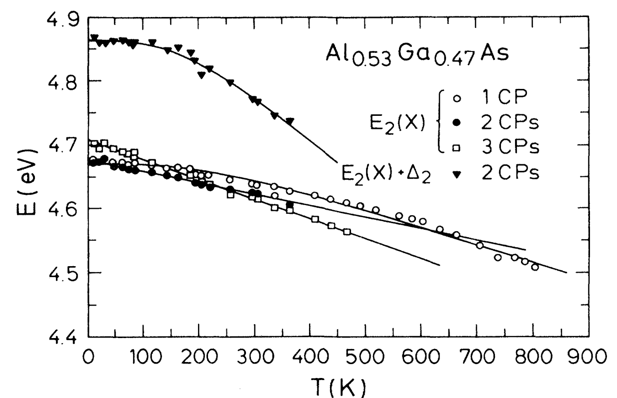

FIG. 13. Temperature dependence of the $E_2(X)$ and $E_2(X)+\Delta_2$ critical-point energies of $Al_{0.53}Ga_{0.47}As$. The solid lines represent fits with either Eq. (2) or a linear expression. The fit parameters are given in Table IV. The results for the $E_2(X)$ structure were obtained by fitting the whole E_2 structure with one CP (open circles), two CP's (solid circles), and three CP's (open squares).

TABLE IV. Parameters obtained by fitting the E_0' and E_2 critical-point energies of $Al_xGa_{1-x}As$ vs temperature to Eqs. (2), (3), and $E(T)=E_L-\gamma T$. For $x=0.69$ we have analyzed the experimental data with both the second- and third-derivative spectra of the dielectric function. The numbers in parentheses indicate error margins.

x	E_B (eV)	a_B (meV)	Θ (K)	$E(0)$ (eV)	α (10^{-4} eV K^{-1})	β (K)	E_L (eV)	γ (10^{-4} eV K^{-1})	Transition	Line shape
0	4.563(21)[a]	59(26)[a]	323(119)[a]	4.509(8)[a]	4.0(7)[a]	241(177)[a]			E_0'	2 CP's
	5.161(33)[a]	38(33)[a]	114(95)[a]	5.133(21)[a]	6.6(4)[a]	43(66)[a]			$E_2(P)$	2 CP's
0.27							4.669(10)	4.91(74)	E_0'	2 CP's
							4.72(10)	4.58(56)	$E_2(X)$	3 CP's
							4.742(6)	3.92(47)	$E_2(X)$	2 CP's
0.53	4.756(23)	86(25)	602(125)	4.672(24)	5.5(9)	1398(700)			$E_2(X)$	1 CP
							4.678(3)	1.82(13)	$E_2(X)$	2 CP's
							4.709(3)	3.12(11)	$E_2(X)$	3 CP's
0.69	5.049(8)	187(84)	491(115)						$E_2(x)+\Delta_2$	3 CP's
	4.784(23)[b]	76(29)[b]	304(80)[b]						$E_2(X)+\Delta_2$	3 CP's
	4.753(11)[c]	47(15)[c]	230(68)[c]	4.712(7)[c]	4.2(3)[c]	130(72)[c]			$E_2(X)$	3 CP's
							4.775(4)[c]	0.93(10)[c]	$E_2(X)+\Delta_2$	3 CP's
				4.867(9)[c]	2.6(2)[c]	188(140)[c]	4.881(7)[c]	2.21(16)[c]	$E_2(\Sigma)$	3 CP's
							4.792(8)[b]	1.64(25)[b]	$E_2(X)+\Delta_2$	3 CP's
							4.866(11)[b]	−0.09(30)[b]	$E_2(\Sigma)$	3 CP's

[a]Reference 24.
[b]For the analysis of the experimental data we used the second-derivative spectra of the dielectric function.
[c]We used the third-derivative spectra of the dielectric function.

TABLE V. Parameters involved in the temperature dependence of the broadening of the E_0' and E_2 critical-point broadenings of $Al_xGa_{1-x}As$. For $x=0.69$ we have analyzed the experimental data with both the second- and third-derivative spectra of the dielectric function. The numbers in parentheses indicate error margins.

x	Γ_1 (meV)	Γ_0 (meV)	Θ (K)	Γ_L (meV)	γ (10^{-4} eV K^{-1})	Transition	Number of CP's
	$-255(19)$[a]	300(123)[a]	1013(218)[a]			E_0'	1
0				84(8)[a]	2.28(19)[a]	E_0'	1
				201(8)	0.68(50)	E_0'	2
				149(7)	2.22(39)	$E_2(X)$	3
0.27				38(3)	0.91(27)	$E_2(X)$	2
				108(3)	169(7)	$E_2(X)$	1
	26(24)	71(26)	365(91)			$E_2(X)$	3
0.53				37(2)	0.36(10)	$E_2(X)+\Delta_2$	3
0.69	$-155(77)$[b]	212(79)[b]	792(145)[b]			$E_2(X)$	3
	103(42)[c]	176(45)[c]	828(127)[c]			$E_2(X)$	3

[a]Reference 24.
[b]For the analysis of the experimental data we used the second-derivative spectra of the $\epsilon(\omega)$.
[c]We used the third-derivative spectra of the $\epsilon(\omega)$.

perature dependence is given in Refs. 4 and 19. For temperatures higher than 250 K the broadening of the doublet components is larger than their splitting. Thus the structure must be treated as a single CP. Table I gives the parameters obtained by fitting the energy E_0 of this CP to Eqs. (2) and (3). From the data in Table I the following compositional dependence of the parameters which describe the temperature dependence can be obtained:

$$E(0)=1.517+1.39x \quad (\text{eV}) , \tag{7a}$$

$$\alpha=5.5+3.35x \quad (10^{-4}\ \text{eV/K}) , \tag{7b}$$

$$\beta=225+88x \quad (\text{K}) , \tag{7c}$$

$$E(B)=1.571+1.49x \quad (\text{eV}) , \tag{7d}$$

$$a_B=57+94x \quad (10^{-4}\ \text{eV}) , \tag{7e}$$

$$\Theta=240+160x \quad (\text{K}) . \tag{7f}$$

The compositional dependence of α [Eq. (7b)] and Θ [Eq. (7f)] is plotted in Fig. 14.

The $E_0+\Delta_0$ (Γ_7 to Γ_6) transitions are much weaker and broader than their E_0 counterparts. Hence we were able to analyze this structure in the $Al_xGa_{1-x}As$ samples only up to 500 K. The parameters obtained by fitting the temperature dependence of the CP energies are listed in Table I.

From the energies of the E_0 and $E_0+\Delta_0$ structures the compositional dependence of the spin-orbit splitting can be obtained: $\Delta_0=337(6)-23(10)x$ meV. No trace of a quadratic dependence on x was found within the scatter of the points.

In the following we discuss the broadening of the E_0 and $E_0+\Delta_0$ structures (Fig. 7 and Table II) in the $Al_xGa_{1-x}As$ alloys.

In Table II the parameters obtained by fitting the broadening of the E_0 and $E_0+\Delta_0$ transitions of $Al_xGa_{1-x}As$ to Eqs. (4) and (5) are listed, together with the corresponding value for the E_0 transition of GaAs. For the data in the Table, the broadening parameters that were obtained from fitting spectra taken with a 5-meV-wide energy step were used. This energy step is too large for analyzing the E_0 structure in $Al_xGa_{1-x}As$ at temperatures below 200 K. Thus the deviations observed in Fig. 7 between the parameters obtained from spectra with a 5-meV energy step with those from spectra with a 1- or 2-meV energy step are due to this artifact. However, the spectra with the 5-meV energy step allows us to describe the E_0 structure with the same model line shape for all

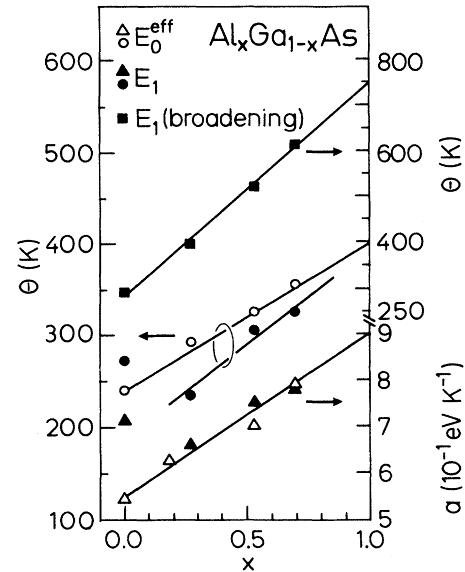

FIG. 14. Compositional dependence of the average phonon frequency Θ [Eq. (2)] and the parameter α [Eq. (3)]. (○,△) and (●,▲) represent results obtained from the analysis of the energies of the E_0 and E_1 transitions of $Al_xGa_{1-x}As$, respectively; ■ represents results obtained from the E_1 broadening. The solid lines represent fits with a linear expression.

the Al compositions over the whole temperature range, as well as to compare the results for E_0 with those for $E_0+\Delta_0$. The data of Fig. 7 show an increase of the E_0 broadening with increasing Al content. The reasons are twofold: (a) as the Al content increases in $Al_xGa_{1-x}As$ the exciton structure broadens due to alloy scattering and (b) for Al content larger than or equal to 0.45 an overlap of E_0 with indirect $\Gamma \rightarrow X$ transitions takes place which increases the broadening of the E_0 structure through phonon and disorder-aided decay into $\Gamma \rightarrow X$ excitations. At low Al content the homogeneous broadening of the E_0 exciton is practically zero for zero temperature and the observed broadening is due to statistical fluctuations of the alloy composition. In Fig. 15 we plot the compositional dependence of the E_0 (solid triangles) and $E_0+\Delta_0$ (solid circles) broadenings that were found from our analysis at low temperatures. In this figure we also plot results from our photoluminescence measurements for $x<0.35$ and Raman results for $x>0.45$ for the E_0 exciton[18] and $x<0.1$ for the $E_0+\Delta_0$ structure.[16] The dashed line in this figure represents the calculated broadening according to Eq. (6). The solid lines are drawn as a guide to the eye.

Figure 7 indicates that the temperature dependence of the E_0 broadening is well described within the scatter by a linear relationship [Eq. (5)]. Not enough information is available to obtain significant parameters for the more physically meaningful Eq. (4). Note that for $x=0.53$ and 0.69 the term n_B in Eq. (4) has been replaced with $2n_B+1$ since now both phonon absorption and emission processes can take place. In the case of $Al_{0.27}Ga_{0.73}As$, even though we could analyze the E_0 and $E_0+\Delta_0$ only up to 350 K, a linear dependence seems to describe the observed broadening versus temperature.

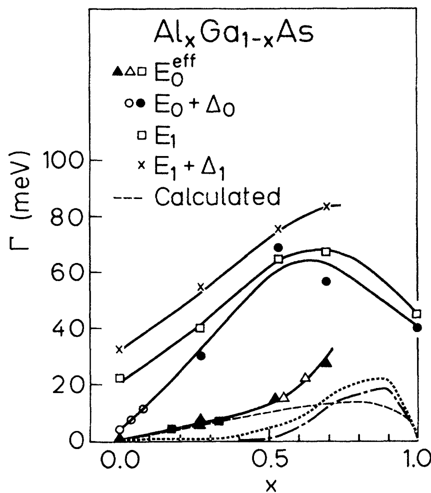

FIG. 15. Compositional dependence of the broadening Γ of the interband transitions found at low temperatures in $Al_xGa_{1-x}As$: broadening of the E_0 exciton (▲) from ellipsometry (SE), from Raman results after Ref. 18 (△) and photoluminescence (PL) measurements (■); broadening of the $E_0+\Delta_0$ transition from SE (●) and from Raman results after Ref. 16 (○); broadening of the E_1 transition (□) from SE; broadening of the $E_1+\Delta_1$ transitions (×) from SE. Solid lines are drawn as a guide to the eye. The dashed line represents the calculated alloy broadening according to Eq. (6). The dotted and dashed-dotted lines have been calculated for alloy scattering using perturbation theory and the CPA, respectively (Ref. 56).

We should mention here that for the $E_0+\Delta_0$ broadening in $Al_xGa_{1-x}As$ at low temperature only a small contribution to Γ_1 or Γ_L is due to alloy broadening, whereas the main contribution is essentially determined by the lifetime of the hole in the split-off band. This is due to the fact that holes in that band near the Γ point have more decay channels than holes in the v_1 (heavy-hole) and v_2 (light-hole) bands.

B. E_1 and $E_1+\Delta_1$ transitions

The E_1 and $E_1+\Delta_1$ peaks in GaAs and AlAs are due to transitions from the upper two valence bands to the lower conduction band,[22,23] the main contribution to the E_1 and $E_1+\Delta_1$ transitions coming from the Λ direction of the BZ, although a region in the ΓLK plane[22] gives also a significant contribution to the corresponding ε_2 (the critical points, emphasized by the derivative spectra, are localized along Λ). Band-structure calculations[22,36] and experimental[25–29] work indicated that the E_1 and $E_1+\Delta_1$ transitions in other III-V compounds and group-IV materials also take place along Λ. A detailed analysis of the line shape of the E_1 and $E_1+\Delta_1$ transitions in GaAs has been performed in Ref. 24; these transitions are best represented below room temperature by a Fano-modified Lorentzian line shape, whereas at higher temperatures a 2D line shape gives a better description of the measurements. The 2D or 3D character of these CP's have also been investigated ellipsometrically versus temperature for Ge,[25] α-Sn,[26] InSb,[28] and InP.[29] At all temperatures, the best fit was found with a 2D CP, although the phase angle ϕ in Eq. (1) at low temperatures has a large value of about 100°. The same situation holds for our fits of the E_1 and $E_1+\Delta_1$ transitions of $Al_xGa_{1-x}As$. In view of this and also for reasons to be discussed later, we have used a 2D line shape to describe the E_1 and $E_1+\Delta_1$ structures.

In Fig. 4 we show the second-derivative spectra of the dielectric function versus energy in the E_1 spectral region for $Al_xGa_{1-x}As$ at low temperatures. The solid and dashed lines represent fits with a 2D CP. We can see that except for the upper wing of the E_1 structure in $Al_{0.27}Ga_{0.73}As$, the 2D representation of the E_1 transitions is wholly suitable to describe the experimental line shape at low temperatures. We have been able to fit simultaneously the E_1 and $E_1+\Delta_1$ CP's up to 760 K for $x=0.27$, 400 K for $x=0.53$, and 300 K for $x=0.69$. In Table III we have listed the parameters obtained by fitting the critical-point energies versus temperature with Eqs. (2) and (3). We can see an increase in Θ, α, and β with increasing Al content. Unfortunately, we cannot compare these parameters with the corresponding ones of GaAs (also shown in Table III) since the GaAs E_1 and $E_1+\Delta_1$ results were obtained by fitting the derivative spectra with a Lorentzian exciton up to 300 K and a 2D

line shape between 300 and 760 K.[24] The same situation is observed for the parameter Θ (see Table VI) obtained by fitting the temperature dependence of the E_1 broadening of $Al_xGa_{1-x}As$ with Eq. (4). The Θ parameter found from the energy shift of the E_1 transition does not have to be necessarily the same as the one found from the broadening. Calculations of the electron-phonon spectral functions for Si, Ge,[31] and GaAs (Ref. 32) have shown that acoustical as well as optical phonons contribute to the energy shifts due to electron-phonon interaction, whereas for the broadening of the E_1 CP mainly optical phonons are responsible. Thus one would expect a higher average phonon frequency Θ from the fit of Eq. (4) to the broadening parameters than for the electron-phonon contributions of the energy shift with temperature. This fact is confirmed by comparing the values Θ of the E_0 and E_1 transitions listed in Tables I and III (i.e., the energy shifts) to those listed in Tables II and VI (i.e., the broadenings), respectively (see also Fig. 14). The Debye temperature[1,47] as well as the mean frequency of phonons[1,18,47] taking part in the scattering process increase in going from GaAs to AlAs. If the parameter Θ from our fits is related to these quantities, it should increase by similar amounts. A linear dependence of the parameter α in Eq. (3) is shown in Fig. 14 for both the E_0 and E_1 transition with increasing Al content.

The temperature dependence of the E_1 and $E_1+\Delta_1$ CP's broadening obtained from the 2D fit is displayed in Fig. 9; in the case of the $E_1+\Delta_1$ CP it is practically linear. The broadening of an electronic state is roughly proportional to the electronic density of states at its energy.[31] Thus the broadening of $E_1+\Delta_1$ transitions should be at least as large as that for E_1 since for the lower split-off valence band there is a larger electronic density of states than for the upper one. This conjecture is borne out by comparing the E_1 and $E_1+\Delta_1$ broadenings of $Al_xGa_{1-x}As$ at low temperatures (LT) in Fig. 9. However, we can see in this figure that a crossover of the E_1 and $E_1+\Delta_1$ broadenings occurs at high temperatures. The $E_1+\Delta_1$ broadening increases more slowly with increasing temperature than the E_1 broadening. A noteworthy decrease (increase) in the temperature dependence of the $E_1+\Delta_1$ (E_1) broadening is observed with increasing Al content. Also, the crossing of the E_1 and $E_1+\Delta_1$ broadenings occurs at lower temperatures with increasing Al content. Since this doublet arises from the spin-orbit splitting of the valence band, it is generally presumed that both structures arise from transitions in the same region of k space and thus the temperature dependence of their widths should be similar. We thus tend to believe that the crossings observed in Fig. 9 are artifacts of the fit resulting from not being able to separate E_1 and $E_1+\Delta_1$ transitions when sufficiently broadened.

Amplitudes for 2D E_1 and $E_1+\Delta_1$ transitions of zinc-blende materials can be estimated within the one-electron approximation by[48,49]

$$A_{E_1}=\frac{44(E_1+\Delta_1/3)}{a_0E_1^2}\,, \tag{8a}$$

$$A_{E_1+\Delta_1}=\frac{44(E_1+2\Delta_1/3)}{a_0(E_1+\Delta_1)^2}\,, \tag{8b}$$

where the lattice constant a_0 is in Å and the energies E_1 and Δ_1 in eV. In Table VII we display the amplitudes A_{E_1} and $A_{E_1+\Delta_1}$ that were calculated according to Eqs. (8) as well as the energies found from our fits at low and room temperature. The amplitudes and the phase angle of the E_1 and $E_1+\Delta_1$ transitions obtained from the 2D line-shape fits versus temperature are shown in Figs. 10 and 11. In these figures the corresponding parameters of GaAs (Ref. 24) are also displayed (dashed lines). The amplitudes of the E_1 CP (see Fig. 10) are nearly constant: (a) over the whole temperature range for $x=0.69$, (b) $T>100$ K in the case of $x=0.53$, (c) $T>200$ K for $x=0.27$, and (d) $T>300$ K in the case of GaAs. These facts indicate a change in the character of the E_1 transitions which takes place at lower temperatures as the Al content increases. This change is also supported when looking at the phase angle (see Fig. 11). A phase angle smaller than 90° is obtained in the above constant amplitude temperature range.

According to Ref. 24 the E_1 and $E_1+\Delta_1$ transitions in GaAs are an example for the coexistence of local and

TABLE VI. Values of the parameters obtained by fitting the broadening Γ of the E_1 and $E_1+\Delta_1$ critical points of $Al_xGa_{1-x}As$ vs temperature to the equation $\Gamma(T)=\Gamma_1+\Gamma_0(2n_B+1)$ or $\Gamma(T)=\Gamma_L+\gamma T$. The numbers in parentheses indicate error margins.

	x	Γ_1 (meV)	Γ_0 (meV)	Θ (K)	Γ_L (meV)	γ (10^{-4} eV K^{-1})	Line shape	Temperature range (K)
					$-19(6)^a$	$1.34(11)^a$	2D	300–760
	0	0(fixed)^a	$41(3)^a$	$293(26)^a$			Excitonic	20–300
	0.27	4.4(4.0)	36.8(5.7)	399(47)			2D	15–700
E_1	0.53	−4.3(5.0)	71(16)	525(89)			2D	12–800
	0.69	−52(37)	123(40)	620(138)			2D	16–750
		0(fixed)^a	$36(1)^a$	$356(17)^a$			Excitonic	20–300
	0				$31(8)^a$	$1.34(15)^a$	2D	300–760
	0.27				53(2)	1.12(5)	2D	15–600
$E_1+\Delta_1$	0.53				74(1)	0.71(7)	2D	12–450
	0.69	51(50)	137(80)	826(600)	80(4)	0.74(15)	2D	16–350

^{a}Reference 24.

TABLE VII. Parameters used to calculate the amplitudes A_{E_1} and $A_{E_1+\Delta_1}$ according to Eqs. (8), together with the experimental amplitudes at low and room temperature.

x	Temperature (K)	a_0 (Å)	E_1 (eV)	$E_1+\Delta_1$ (eV)	Δ_1 (meV)	A_{E_1}	$A_{E_1+\Delta_1}$
	20		3.038(1)[a]	3.262(2)[a]	224[a]	7.3	3.26
0	RT	5.6535[b]	2.915(2)[a]	3.139(3)[a]		4.6	3.3
						2.8[c]	2.5[c]
	15		3.2255(14)	3.4393(47)	219	5.6	3.6
0.27	RT	5.6554[b]	3.104(2)	3.309(6)	205	4.5	3.1
						2.6[c]	2.3[c]
	12		3.3869(13)	3.5796(36)	193	5.4	3.4
0.53	RT	5.6574[b]	3.2630(21)	3.4708(48)	208	4.4	1.9
						2.4[c]	2.2[c]
	16		3.5354(31)	3.7226(84)	187	3.8	2.7
0.69	RT	5.6587[b]	3.4064(71)	3.6085(120)	202	3.9	1.7
						2.3[c]	2.1[c]
	80		3.994(2)	4.132(10)	138		
1	RT	5.6611[b]	3.899[d]	4.048[d]	149[d]	7.1	
						2.02[c]	1.9[c]

[a]Reference 1 obtained by linear interpolation $[a_0(x)=5.6535+0.0078x]$ at room temperature.
[b]Reference 24.
[c]Calculated amplitudes at room temperature, small differences exist with the corresponding ones at low temperatures.
[d]Reference 38.

band characters in the optical spectra of solids (see for example Ref. 48). Thus for $T<300$ K in GaAs these two structures could be described by a quasilocal state superimposed upon a background of continuous states which leads to Fano-Breit-Wigner interference effects. For temperatures above 300 K, the line shape of the E_1 and $E_1+\Delta_1$ CP's in GaAs is better described with a 2D line shape according to Eq. (1). The phase angle ϕ in this expression describes the metamorphism of critical-point line shapes due to excitonic effects by allowing a continuous admixture between two adjacent CP's.[50] In the case of 2D critical points this limits ϕ to the range 0°–270°. However, when the E_1 structure is treated as an uncorrelated one-electron transition it should correspond to interband minima and the phase angle is further restricted to the range $0°<\phi<90°$. As already discussed, in the case of $Al_xGa_{1-x}As$ with $x=0.27$ and 0.53 and for temperatures smaller than 200 and 100 K, respectively, we have found a situation similar to that for GaAs. Thus the coexistence of local and band character also occurs in the E_1 and $E_1+\Delta_1$ CP's of the $Al_xGa_{1-x}As$ system. However, the quasilocal character shifts to lower temperatures, as soon as the Al content increases, and disappears around $x=0.6$ becoming strong again for AlAs. Correspondingly, the values of A_{E_1} calculated with Eq. (8a) agree better with the experimental ones for $x=0.53$ and 0.69 than for $x=0$ and 1. This is also supported by the E_1 and $E_1+\Delta_1$ broadenings found at low temperatures. For example, Fig. 15 shows that the compositional dependence of the E_1 and $E_1+\Delta_1$ broadenings is similar to that described by Eq. (6). It is obvious that alloying considerably increases the intrinsic broadening of the E_1 and $E_1+\Delta_1$ transitions with increasing x, until x reaches a value between 0.7 and 0.8 and then decreases again. Thus the broadening of these two transitions may be partly due to the suppression of excitonic effects with alloying. A similar asymmetric compositional dependence of the broadening of E_1 and $E_1+\Delta_1$ structures was found from ellipsometric measurements at room temperature in the $Cd_xHg_{1-x}Te$ system.[51] The maximum in the compositional dependence of the E_1 and $E_1+\Delta_1$ broadening in $Cd_xHg_{1-x}Te$ was found at $x=0.8$, a bit higher maximum ($x=0.9$) having been found from photoluminescence measurements of the exciton broadening in $Cd_xHg_{1-x}Te$.[52]

The coherent-potential approximation (CPA) provides a theoretical framework which can be used to study alloys in the case of relatively weak disorder. In Ref. 53 by using the CPA a measure of the scattering strength δ for band-edge electrons due to alloy disorder in $Cd_xHg_{1-x}Te$ was obtained. The disorder in $Cd_xHg_{1-x}Te$ manifests itself primarily in the difference of cation s-level energies associated with relativistic shifts. The s character of the higher conduction bands above 2 eV and the valence bands below about -5 eV show effects associated with strong disorder. The alloy scattering broadening in the conduction and valence bands along the Λ direction was found to be about 3 times stronger in the Cd-rich than in the Hg-rich region. This result is in agreement with the increased broadening reported in Ref. 51 for the Cd-rich region. It is also found in Ref. 53 that the alloy scattering lifetime is stronger in the first conduction band than in the two uppermost valence bands. As mentioned in Ref. 51, a possible explanation for the asymmetry observed in the E_1 and $E_1+\Delta_1$ broadening of $Cd_xHg_{1-x}Te$ is that for larger x the final states involved in the E_1 transitions lie in an energy region where the minority component has a large density of states giving a larger alloy

broadening. In Ref. 54 (see also Ref. 9) it has been found that for $GaP_{0.5}As_{0.5}$ the alloying lifetime broadening is much larger in the upper valence bands along both Λ and Δ directions than in the lowest conduction band with the exception of the Γ point.

CPA calculations have also been performed for $Al_xGa_{1-x}As$ alloys.[55,56] We show in Fig. 15 the results of CPA calculations (dashed-dotted line), as well as those of second-order perturbation theory calculations involving the full pseudopotential difference (dotted line).[56] It is interesting to note that they both describe well the increase in Γ above the band crossing point ($x \approx 0.5$) but not below it. The sum of these results plus the contribution of concentration fluctuations to the excitonic energy [Eq. (6), dashed line in Fig. 15] seems to give an excellent description of the measured $\Gamma(x)$.

A related feature is also displayed in Fig. 16. The phase angle of the E_1 and $E_1+\Delta_1$ transitions in Fig. 16(a) shows a minimum (lowest excitonic effects) around $x=0.7$, which is likely to be related to the behavior of the E_1 and $E_1+\Delta_1$ broadening (Fig. 15). It is obvious from Fig. 16 that the phase angle has the same compositional dependence at low and room temperature. In the case of the strength A [Fig. 16(b)] a similar compositional dependence for the E_1 transitions appears at 16 K and room temperature.

The amplitudes calculated according to Eqs. (8) [solid lines in Fig. 16(b)] are on the average about half the experimental ones (note, however, that they become closer for $x \approx 0.6$, as mentioned above). This fact has been also found in most group-IV and III-V materials. Calculations for Si (Refs. 57 and 58) and GaAs,[59] by taking into account a correction for the terms linear in k for k perpendicular to $\langle 111 \rangle$, increase the strength of the E_1 structure relative to $E_1+\Delta_1$. However, this effect should be small ($\sim 20\%$) for our materials.[59] A portion of the observed differences in the absolute magnitude of calculated and experimental A_{E_1} can also be attributed to excitonic interaction.[60,61]

We have obtained, for the compositional dependence of the Δ_1 spin-orbit splitting (in meV) at low temperature and room temperature (RT) by fitting the experimental results with either linear or quadratic expressions,

$$\Delta_1 = \begin{cases} 233(20)-83(30)x \\ 223(21)-10(40)x-74(40)x^2 \end{cases} \text{at LT} \quad \begin{cases} 229(30)-64(40)x \\ 218(30)+23(50)x-87(80)x^2 \end{cases} \text{at RT} . \tag{9}$$

A negative bowing parameter (coefficient of x^2) is found, in agreement with other alloy systems.[11,62] The difference in bowing parameter found between LT and RT is not significant in view of the error margins.

It has been suggested[63] that the Δ_1 spin-orbit splitting can be predicted from the spin-orbit splitting Δ_{at} of the separate atoms from which the alloy $A_x^{III}B_{1-x}IIIC^V$ is formed according to relation

$$\Delta_1 = a_1 - c_1 x^2 ,$$
$$c_1 = a_\Delta[\Delta_{at}^{III}(B) - \Delta_{at}^{III}(A)] , \tag{10}$$

where $a_\Delta = \frac{2}{8}$.

For comparison with Eq. (9), values of Δ_{at} have been taken to be Ga=170 meV and Al=20 meV. The calculated $c_1 = 56$ meV is in good agreement with that of Eq. (9).

C. E_0' and E_2 transitions

The nature of the E_2 transitions is more complicated since they do not correspond to a single, well-defined CP. The strong structures observed in GaAs (see Fig. 5) have been identified as E_0' at 4.5 eV and $E_2(\Sigma)$ at 5.12 eV.[24,37] The E_0' structure corresponds to transitions in the vicinity of the Γ point ($\Gamma_8 \rightarrow \Gamma_7$), whereas $E_2(\Gamma)$ has been attributed to transitions in a wide region of the ΓXUL plane.[22,36] Also several weaker structures have been observed in the low-temperature electroreflectance[37] and el-

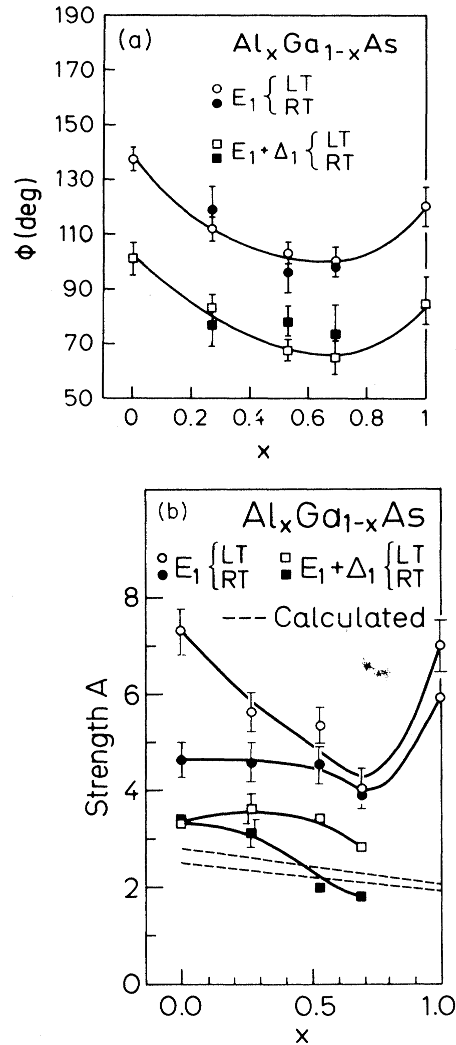

FIG. 16. Compositional dependence of (a) the phase angle ϕ and (b) the strength A of the E_1 and $E_1+\Delta_1$ transitions of $Al_xGa_{1-x}As$. The solid lines in (a) and the dashed ones in (b) are plotted as a guide to the eye. The solid lines in (b) represent the calculated E_1 and $E_1+\Delta_1$ strengths according to Eq. (8).

lipsometry[24] spectra of GaAs. These structures have been identified as two groups of transitions.[37] One group corresponds to transitions at and close to Γ in the Δ direction [$E'_0(\Delta)$ and $E'_0+\Delta'_0$] and the other group has been assigned to transitions in the Δ direction near the X point [$E_2(X)$ and $E_2(X)+\Delta_2$]. In a recent paper[34] we have modified the previous assignment and notation, which led to some difficulties, and have extended it to the whole $Al_xGa_{1-x}As$ range. Thus the strongest structure in GaAs coming from transitions in the ΓXUL plane is called $E_2(P)$, the weaker transitions at X ($X_7 \rightarrow X_6$) or near it ($\Delta_5 \rightarrow \Delta_5$) are called $E_2(X)$ whereas the transitions around the K point are called $E_2(\Sigma)$. We have found that the main changes in the electronic structure of $Al_xGa_{1-x}As$ alloy occur at low Al content. For instance, the shift of E'_0 to higher energies and that of E_2 of about 200 meV to lower energies as well as the appearance of the $E_2(X)$ ($\Delta_5 \rightarrow \Delta_5$) transitions are already observable in $Al_{0.27}Ga_{0.73}As$ (Fig. 5).

The complicated structure around E_2 in GaAs, which extends over the 4.4–5.2-eV energy range, becomes in $Al_xGa_{1-x}As$ more complex since now the $\Delta_5 \rightarrow \Delta_5$ transitions appear and all the transitions take place in the reduced energy range from 4.6 to 5.0 eV. To analyze this region, we have performed a fit of the second-derivative spectra assuming up to five structures in $Al_xGa_{1-x}As$. Unfortunately we could not resolve the E'_0 structure for $x > 0.27$ (it seems to disappear). A comparison of these results with band-structure calculations suggested[34] that the separation $\Delta_5 \rightarrow \Delta_5$ is almost constant over a large portion of the Δ direction whereas the same separation increases near the Γ point when going from GaAs to AlAs. Therefore the E'_0 transition in $Al_xGa_{1-x}As$ is expected to be at nearly the same energies as the $E_2(X)$ and $E_2(X)+\Delta_2$ transitions. With increasing temperature the sharp features of the low-temperature spectra smear out and the weak structures can no longer be resolved even in the derivative spectra.

We have chosen the 2D line shape to fit the experimental data over the whole temperature range in $Al_xGa_{1-x}As$. For $x = 0.27$ two different models were used. Figure 12 shows the temperature dependence of the energies obtained with a model with two critical points E'_0 and $E_2(X)$, as well as the values for $E_2(X)$ obtained when a model with three CP's, E'_0, $E_2(X)$, and $E_2(X)+\Delta_2$ was used.

An energy difference of about 25 meV was found between the two procedures. The spectra of $Al_{0.53}Ga_{0.47}As$ show two main features [$E_2(X)$ and $E_2(X)+\Gamma_2$]. The derivative spectra were analyzed with three different models assuming either one, two, or three 2D critical points. The results are displayed in Fig. 13. Finally, the spectra of the $x = 0.69$ alloy show three main structures, $E_2(X)$, $E_2(X)+\Delta_2$, and $E_2(\Sigma)$. Most of the energies and broadenings of the fitted CP's show a linear dependence with temperature (Figs. 12 and 13). The parameters obtained by fitting the temperature dependence of energies and broadenings with a linear expression or with Eqs. (2)–(4) are given in Tables IV and V.

We should mention that the large broadenings found for the E'_0 and $E_2(X)$ structures in $Al_xGa_{1-x}As$ for $x = 0.27$ are artifacts of the shift of E'_0 transitions to higher energies, since a number of weak structures contribute in this region. For $x = 0.69$ E'_0 seems to coincide with $E_2(X)$ while in the case of AlAs the E'_0 seems to occur close to the $E_2(X)+\Delta_2$ structure. This is in agreement with the increase in the strength A of the $E_2(X)$ or $E_2(X)+\Delta_2$ structures as the E'_0 is shifted to higher energies (see also Fig. 6 in Ref. 34).

V. CONCLUSIONS

We have measured the temperature dependence of the dielectric function of three $Al_xGa_{1-x}As$ alloys by means of spectroscopic ellipsometry in the 1.4–5.6-eV region from 12 to 800 K. By performing a line-shape analysis of the structures observed, the parameters of the E_0 exciton and the $E_0+\Delta_0$, E_1, $E_1+\Delta_1$, E'_0, $E_2(X)$, and $E_2(X)+\Delta_2$ critical points were obtained as a function of temperature. An analysis of the E_1 transitions shows a systematic change in the character of these transitions from a localized Lorentzian in GaAs to a 2D character modified by the electron-phonon interaction, both with increasing Al content and temperature. Large changes are observed around the E'_0 and E_2 structures in the $Al_xGa_{1-x}As$ samples with low Al content. At higher Al concentrations the changes are not so drastic but in this compositional regime contributions from the two upper valence bands to the two lower conduction bands occur in a limited energy range, a fact which increases the complexity of the structure observed around E_2. An attempt was made to analyze the main transitions that occur in this energy region versus temperature, while a detailed analysis of the whole structure was made only at low temperatures.

A strong weakening of excitonic effects in the E_0, $E_0+\Delta_0$, and E_1 transitions of the $Al_xGa_{1-x}As$ alloys was found to occur due to statistical fluctuations of the alloy composition. The effect of these fluctuations also appears as an additional inhomogeneous broadening in the CP's of $Al_xGa_{1-x}As$. For $x \simeq 0.5$ it yields the main contribution to the broadenings at low temperatures where the thermal broadenings are small. The temperature dependence of the energy shift and broadening of the E_0, $E_0+\Delta_0$, E_1, and $E_1+\Delta_1$ transitions as well as a number of transitions around the E_2 region was obtained for various Al compositions and compared with those of GaAs. The compositional dependence of the parameters involved in the temperature dependence of CP's was also obtained. It can be extrapolated to AlAs, a material difficult to measure versus temperature.

ACKNOWLEDGMENTS

One of us (S.L.) acknowledges financial support from the Alexander von Humboldt Foundation. The $Al_xGa_{1-x}As$ samples used were kindly given to us by E. Bauser and the AlAs by K. Ploog. We thank M. Alouani for the band-structure calculations of GaAs and AlAs and L. Tapfer for the x-ray determination of the alloy composition. Also, we would like to thank H. Hirt, M. Siemers, and P. Wurster for their expert technical assistance.

*Permanent address: Department of Physics, Aristotle University of Thessaloniki, 54006 Thessaloniki, Greece.

[1]S. Adachi, J. Appl. Phys. **58**, R1 (1985).
[2]G. A. Rozgonyi, P. M. Petroff, and M. B. Panish, J. Cryst. Growth **27**, 106 (1974).
[3]G. H. Olsen, C. J. Neusse, and R. T. Smith, J. Appl. Phys. **49**, 5523 (1978).
[4]S. Logothetidis, M. Cardona, L. Tapfer, and E. Bauser, J. Appl. Phys. **66**, 2108 (1989).
[5]H. C. Casey and M. B. Panish, *Heterostructure Lasers* (Academic, New York, 1978), p. 193.
[6]C. Bosio, J. L. Staehli, M. Guzzi, G. Burri, and R. A. Logan, Phys. Rev. B **38**, 3236 (1988).
[7]H. J. Lee, L. Y. Juravel, J. C. Woolley, and A. J. Spring Thorpe, Phys. Rev. B **21**, 659 (1980).
[8]A. K. Saxena, Phys. Status Solidi B **105**, 777 (1981).
[9]A. B. Chen and A. Sher, Phys. Rev. B **23**, 5360 (1981).
[10]M. F. Ling and D. J. Miller, Phys. Rev. B **38**, 6113 (1988).
[11]O. Berolo and J. C. Woolley, Can. J. Phys. **49**, 1335 (1974).
[12]D. E. Aspnes, S. M. Kelso, R. A. Logan, and R. Bhat, J. Appl. Phys. **60**, 754 (1986).
[13]B. Monemar, K. K. Smith, and G. D. Pettit, J. Appl. Phys. **47**, 2604 (1976).
[14]P. Omling, L. Samuelson, and H. G. Grimmeiss, J. Appl. Phys. **54**, 5117 (1983).
[15]E. F. Schubert, E. O. Gobel, Y. Horikoshi, K. Ploog, and H. J. Queisser, Phys. Rev. B **30**, 813 (1984).
[16]W. Kauschke, M. Cardona, and E. Bauser, Phys. Rev. B **35**, 8030 (1987).
[17]V. I. Gavrilenko, C. Trallero-Giner, M. Cardona, and E. Bauser, Solid State Commun. **67**, 459 (1988).
[18]C. Trallero-Giner, V. I. Gavrilenko, and M. Cardona, Phys. Rev. B **40**, 1238 (1989).
[19]S. Logothetidis, M. Cardona, and C. Trallero-Giner, J. Appl. Phys. **67**, 4133 (1990).
[20]M. Cardona, *Modulation Spectroscopy* (Academic, New York, 1969), Suppl. 11.
[21]D. E. Aspnes, in *Handbook on Semiconductors,* edited by M. Balkanski (North-Holland, Amsterdam, 1980), Vol. 2, p. 109.
[22]M. Alouani, L. Brey, and N. E. Christensen, Phys. Rev. B **37**, 1167 (1988).
[23]D. E. Aspnes and A. A. Studna, Phys. Rev. B **27**, 985 (1983).
[24]P. Lautenschlager, M. Garriga, S. Logothetidis, and M. Cardona, Phys. Rev. B **35**, 9174 (1987), and references therein.
[25]L. Viña, S. Logothetidis, and M. Cardona, Phys. Rev. B **30**, 1979 (1984).
[26]L. Viña, H. Höchst, and M. Cardona, Phys. Rev. B **31**, 958 (1985).
[27]P. Lautenschlager, M. Garriga, L. Viña, and M. Cardona, Phys. Rev. B **36**, 4821 (1987).
[28]S. Logothetidis, L. Viña, and M. Cardona, Phys. Rev. B **31**, 947 (1985).
[29]P. Lautenschlager, M. Garriga, and M. Cardona, Phys. Rev. B **36**, 4813 (1987).
[30]P. B. Allen and M. Cardona, Phys. Rev. B **27**, 4760 (1983).
[31]P. Lautenschlager, P. B. Allen, and M. Cardona, Phys. Rev. B **33**, 5501 (1986).
[32]S. Gopalan, P. Lautenschlager, and M. Cardona, Phys. Rev. B **35**, 5577 (1987).
[33]S. Zollner, S. Goplan, M. Garriga, J. Humlíček, and M. Cardona, in *Proceedings of the 19th International Conference of Semiconductors, Warsaw, 1988,* edited by W. Zawadzki (Institute of Physics, Warsaw, 1988), Vol. 2, p. 1513.
[34]S. Logothetidis, M. Alouani, M. Garriga, and M. Cardona, Phys. Rev. B **41**, 2959 (1990).
[35]D. D. Sell, Phys. Rev. B **6**, 3750 (1972).
[36]M. L. Cohen and J. R. Chelikowsky, in *Electronic Structure and Optical Properties of Semiconductors,* edited by M. Cardona, Springer Series in Solid State Science Vol. 75 (Springer-Verlag, Berlin, 1988), p. 102.
[37]D. E. Aspnes and A. A. Studna, Phys. Rev. B **7**, 4605 (1973).
[38]M. Garriga, P. Lautenschlager, M. Cardona, and L. Ploog, Solid State Commun. **61**, 157 (1987).
[39]A. Onton, in *Proceedings of the 10th International Conference of the Physics of Semiconductors, Cambridge, Mass., 1970,* edited by S. P. Keller, J. C. Mensel, and F. Stern (U.S. GPO, Washington, DC, 1970), p. 107.
[40]S. Adachi, Phys. Rev. B **38**, 12 345 (1988).
[41]R. M. A. Azzam and N. M. Bashara, in *Ellipsometry and Polarized Light* (North-Holland, Amsterdam, 1977).
[42]D. E. Aspnes, G. P. Schwartz, G. J. Gualtieri, A. A. Studna, and B. Schartz, J. Electrochem. Soc. **128**, 590 (1981).
[43]Y. P. Varshni, Physica (Utrecht) **34**, 149 (1967).
[44]C. Charreaux, G. Guillot, and A. Nouailhat, J. Appl. Phys. **60**, 768 (1986).
[45]F. H. Pollak and M. Cardona, Phys. Rev. **172**, 816 (1968).
[46]M. Chandrasekhar and F. H. Pollak, Phys. Rev. B **15**, 2127 (1977).
[47]*Landolt-Börnstein Tables,* edited by O. Madelung, M. Schulz, and H. Weiss (Springer-Verlag, Berlin, 1982), Vols. 17a and 22a.
[48]M. Cardona, in *Atomic Structure and Properties of Solids* (Academic, New York, 1972), p. 514.
[49]M. Cardona, in *Light Scattering in Solids II,* edited by M. Cardona and G. Güntherodt, Springer Topics in Applied Physics Vol. 50 (Springer-Verlag, Berlin, 1982), p. 19.
[50]Y. Toyozawa, M. Inoue, T. Inui, M. Okazaki, and E. Hanamura, J. Phys. Soc. Jpn. Suppl. **21**, 133 (1966); **22**, 1337 (1967).
[51]L. Viña, C. Umbach, M. Cardona, and L. Vodopyanov, Phys. Rev. B **29**, 6752 (1984).
[52]A. Lusson, R. Legros, Y. Marfaing, and H. Mariette, Solid State Commun. **67**, 851 (1988).
[53]K. C. Hass, H. Ehrenreich, and B. Velický, Phys. Rev. B **27**, 1088 (1983).
[54]S. Sakai and T. Sugano, J. Appl. Phys. **50**, 4143 (1979).
[55]A. B. Chen and A. Sher, Phys. Rev. B **23**, 5360 (1981).
[56]C. Grein (private communication).
[57]M. Cardona, Phys. Rev. B **15**, 5999 (1977).
[58]A. Daunois and D. E. Aspnes, Phys. Rev. B **18**, 1824 (1978).
[59]D. E. Aspnes and M. Cardona, Solid State Commun. **27**, 397 (1978).
[60]W. Hande, in *Advances in Solid State Physics,* edited by J. Treusch (Vieweg, Braunschweig, 1979), Vol. 19, p. 43.
[61]W. Hanke and L. J. Sham, Phys. Rev. B **21**, 4656 (1980).
[62]P. Parayanthal, C. S. Ro, R. H. Pollak, C. R. Stanley, G. W. Wicks, and L. F. Eastman, Appl. Phys. Lett. **43**, 109 (1983).
[63]S. S. Vishnubhata, B. Eyglunent, and J. C. Woolley, Can. J. Phys. **47**, 1661 (1969).